Sustainable Energy Technologies and Assessments 65 (2024) 103776

Contents lists available at ScienceDirect

Sustainable Energy Technologies and Assessments

journal homepage: www.elsevier.com/locate/seta

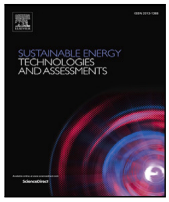

Future offshore wind energy evolution in the Bay of Biscay

Hodei Ezpeleta [a,*], Alain Ulazia [a], Gabriel Ibarra-Berastegi [b,c], Jon Sáenz [c,d], Sheila Carreno-Madinabetia [e], Oihana Aristondo [f]

[a] Department of Energy Engineering, University of the Basque Country (UPV/EHU). Engineering School of Gipuzkoa-Eibar, Spain
[b] Energy Engineering Department, University of the Basque Country (UPV/EHU)., Alda. Urkijo, 48013 Bilbao, Spain
[c] Plentziako Itsas Estazioa, University of the Basque Country (UPV/EHU)., Areatza Hiribidea 47, 48620 Plentzia, Spain
[d] Department of Physics, University of the Basque Country (UPV/EHU)., Leioa, Spain
[e] Department of Mathematics, University of the Basque Country (UPV/EHU)., Paseo de la Universidad, 01006 Vitoria-Gasteiz, Spain
[f] Department of Applied Mathematics, University of the Basque Country (UPV/EHU). Engineering School of Gipuzkoa-Eibar, Spain

ARTICLE INFO

Keywords:
Floating offshore wind energy
CMIP6
ERA5
Long-term energy trends

ABSTRACT

A relevant point near the Biscay Marine Energy Platform (BiMEP) has been chosen and data from the ERA5 reanalysis and CMIP6 datasets in future SSP5-85 scenario (wind and wave data) have been used to analyse the energy potential and its trends from 2015 to 2100 for wind energy. A 15 MW wind turbine has been chosen in line with current technological state-of-the-art and needs, and its energy production has been computed considering the corresponding power curve, and the wind speed at its hub height based on the variation of sea roughness due to the sea state (wave height and period). The results, although most of them have not been relevant, have shown a slightly downward trend mostly on winter in all parameters analysed: mean wave period (T_m), significant wave height (H_s), corresponding sea roughness (z_0), and wind speed at hub height (U_x). The 15MW wind turbine simulation has therefore shown a small decrease in energy production.

Introduction

The ocean renewable energy (ORE) has a huge energy potential to produce electricity with the different combinations of energy resources carried by waves, tides, salinity, and ocean temperature differences, together with offshore wind power. In the last two decades there has been a growing interest in the ocean's energy potential, both for the energy of the waves and for the wind energy, being more laminar and less turbulent offshore than onshore, although operation and maintenance can be more complex [1]. These resources could greatly help achieve the European Union's decarbonization objectives by 2050. The specific targets are 40% global reduction and a net domestic reduction of at least 55% in Greenhouse gases (GHG) emissions by 2030 compared to 1990, and 27% of the total energy production by renewable energy sources [2], using mainly wind energy [3], and different developments of solar energy [4,5]. It should be emphasized that climate neutrality can only be achieved with a boost in renewable energies that also includes ORE [6]. Furthermore, the Commission aims to increase Europe's offshore wind capacity from 12 GW to at least 60 GW by 2030 and 300 GW by 2050 [7], which can be even higher since floating offshore wind could cover 61.55% of the exploitable area using the optimal macroscale substructures [8].

One key issue in grid integration is long term prevision, due to the fact that the wave and wind energies, as with other types of renewable energies, are intermittent [9]. The wave energy, in particular, is difficult to predict because the wave height (H_s) and the wave period (T_p) non-linearity combine by multiplying making the error for the energy flow forecast higher than their forecasts individually, adding to this issue strong historical seasonal variations from winter to summer in locations such as Ireland [10], Iceland [11] or Chile [12].

Given these reasons and because of the need for optimal long-term forecast and investigation in future trends of these intermittent resources, the OREs are getting more and more attention in the recent scientific literature [13]. The present study focuses on the long-term wind and wave parameter trends (2015–2100) at a referential point near the Basque Coast in a marine energy experimental platform, with the aim of reaching a suitable projection of future offshore wind energy production in different climate scenarios in order to take advantage of it.

This experimental location should be analysed in the context of maritime space management plan of Spanish government around the Iberian Peninsula (Bay of Biscay and Mediterranean), and Canary Islands (POEM, *Plan de Ordenación del Espacio Marítimo* [14] 1si, showing a strong potential in the Bay of Biscay, mainly in Galicia and

* Corresponding author.
E-mail address: alain.ulazia@ehu.eus (A. Ulazia).

https://doi.org/10.1016/j.seta.2024.103776
Received 12 December 2023; Received in revised form 16 March 2024; Accepted 14 April 2024
Available online 18 April 2024

List of abbreviations

BIMEP	Biscay Marine Energy Platform
C3S	Copernicus Climate Change Service
CI	Confidence Interval
CSIRO	Commonwealth Scientific and Industrial Research Organisation
DTU	Technical University of Denmark
EU	European Union
ECMWF	European Centre for Medium-Range Weather Forecasts
GHG	Greenhouse Gases
IEA	International Energy Agency
JAS	July, August, September — summer season months
JFM	January, February, March — winter season months
LCOE	Levelized Cost of Energy
MBC	Multivariate Bias Correction of Climate Model Outputs
NREL	National Renewable Energy Laboratory
ORE	Ocean Renewable Energy
OWC	Oscillating Water Column
POEM	Plan de Ordenación del Espacio Marítimo
QM	Quantile-Matching
QMD	Quantile Mapping and Dressing
SSPs	Shared Socioeconomic Pathways

Nomenclature

AEP	Annual Energy Production [kWh]
CF	Capacity Factor [%]
d	Water depth [m]
g	Earth's gravity force acceleration [9.81 m/s^2]
H_s	Significant wave height [m]
L	Peak period wavelength [m]
N	Number of analysed cases per year [2922 cases]
p	Pressure [Pa]
P_{rated}	Nominal power of the turbine [15 MW]
$P(U)$	Power based on the wind speed [kW]
t	Temperature [K]
T_m	Mean wave period [s]
T_p	Peak wave period [s]
U_x	Wind speed at x height [m/s]
WPD	Wind Power Density [W/m^2]
z_0	Sea roughness value [m]
Δt	Time period [3 h]

Asturias [15]. The corresponding Figure-S1 of the supplementary material, shows the main maritime boundaries of POEM emphasizing Canary Islands with trade winds [16], the West of Bay of Biscay with the NW predominant component [17], and the NW of the Mediterranean with also strong N tramuntana winds around the Gulf of Lion [18]. In the next section, Fig. 1 shows more specific details of the selected area in the Basque Country, including bathymetry analysis, where a referential experimental offshore wind farm area will be constituted.

The main novelty of this article is to apply last coordinated CMIP6 future projections with waves, not only wind speed, for future offshore wind energy projections. The novel method considers the instantaneous roughness of the sea depending on wave period and height for the application of the logarithmic law that describes the vertical profile of the wind, and therefore, gives the value of wind speed at hub height of the selected turbine. This is a pioneering approximation procedure, for these reasons:

1. The novelty of data: CSIRO offers future data not only with wind speed, but also with wave data, which is not used in the previous studies with CMIP5 or CMIP6.
2. The use of 3-hourly data to compute the instantaneous power using turbine power curve, and the consequent computation of AEP and CF.
3. The methodological novelty: the use of wave height and period to obtain sea roughness and apply it to the wind vertical profile.

Recent literature applying global CMIP6 projections found a significant decline by 2100 in the mid-latitudes of the Northern Hemisphere. These changes are highly dependant on future climate scenarios [19]. There is a global increase in the variability of Wind Power Density (WPD) [20], though there are more references using CMIP5 and CMIP6 about Europe and North America [21]. A recent work suggests a reliable and stable horizon for the development of offshore wind energy [22].

Most of the previous CMIP6 based literature does not consider the real energy production of the turbine and its capacity factor in the real power curve using hourly data. These articles only study WPD and wind speed evolution: [19,20,23–30]; In these cases, monthly data is used: [26,28,30–32]. That is, previous literature has generally ignored the translation of natural wind energy to real electrical production in long-term and future projection studies.

The article is structured as follows: first, the studied area in the Basque Coast is defined together with the data used from CSIRO and ERA5 reanalysis to calibrate CMIP6 projections data; then, the calibration method and also the characteristics of the 15 MW turbine are described; methodologically, the equations to obtain sea roughness and the application of the log law for the vertical profile of wind are specified to compute the energy production and its future trends; all this combination of data and methods are synthesized in two flux diagrams to visually clarify all the steps for the reader; after that, the results show the validation versus ERA5 of the CMIP6 source and the future wind and wave trends, to finally present the energy production trends of the 15 MW turbine and extreme event behaviour; the Discussion section interprets these results with general connections for global warming and in Conclusions the authors emphasizes the main results and the future outlook of the presented methods.

Data and methodology

Data

The data used here constitute, as far as we know, an unique source for future CMIP6 projections incorporating wave data via an atmosphere-oceanic coupling simulation. According to the original methodology presented here, as it is shown in the next sections, these data about wave period and wave height are essential to obtain the instantaneous roughness of the sea via the Hsu law (Eq. (2)), and to raise the original wind speed at 10 m to the turbine hub height at 150 m using the logarithmic law (Eq. (3)) [33].

Study area

Our gridpoint is located in the Bay of Biscay [Fig. 1-a], at coordinates 43.5°N, 2.5°W. This location has been chosen for its good energetic potential, since it is between Biscay Marine Energy Platform (BIMEP) and the Mutriku's Oscillating Water Column (OWC) (both areas, BIMEP [34] and Mutriku [35] are well studied energetically). It should be underlined that the seabed of the Basque Coast tends to descend deeply a few kilometres from the shore, which supports the future

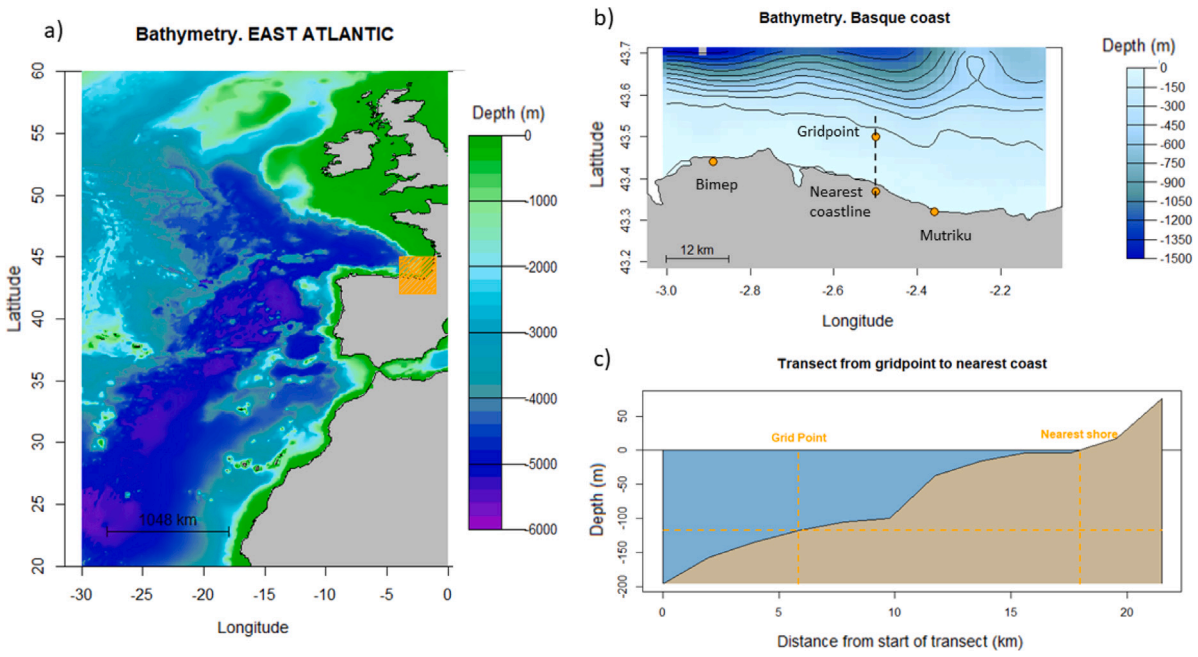

Fig. 1. (a) East Atlantic Sea bathymetry with the studied area in orange. (b) Zoom of the studied area with the most relevant points. (c) Transect from the gridpoint to the coast [39].

prospect of floating wind power installation since the deployment of floating wind turbines in deep waters is favoured by several advantages, such as more stable winds, lower visual impact and flexible acoustic noise requirements [36]. In fact, part of the objective of this study is to check the hypothesis that the projections of the energy resource at the analysed location justifies the installations of such floating wind power devices. Consequently, the grid point is located about 13 km off the Basque coast to the north and at a depth of about 120 m, beyond the prohibitive limit of 10 km imposed by the European Commission [37], and well within the technical limit of anchoring depth of 1000 m [38].

ERA5 reanalysis

ERA5 reanalysis data have been used as a historical base and validation of future projections [40]. For the preparation of ERA5, the European Centre for Medium-Range Weather Forecasts (ECMWF [41]) reprocessed all observations using a frozen data assimilation system (its IFS Earth System model, CY41R2). The data from the reanalysis are distributed by the Copernicus Climate Change Service (C3S) and they currently cover the period from 1940 to the present [42].

The ERA5 reanalysis is the fifth major global reanalysis produced by ECMWF, providing hourly data with a spatial resolution of 0.25° × 0.25° (about 30 km) worldwide for the downloaded meteorological data. For atmosphere and wind energy analysis, wind speed at 10 m (U_{10}), surface pressure (p) and temperature at 2 m (t_2) are used. However, for wave data, the available spatial resolution is 0.5° × 0.5° (about 50 km), and the parameters used are significant wave height (H_s) and mean wave period (T_m) or peak wave period (T_p).

CSIRO: CMIP6, wind and wave

The second data source used in this study is Commonwealth Scientific and Industrial Research Organisation (CSIRO), an ocean wave's climate simulations dataset with its persistent link to share the collection (link [43]). The dataset has been globally validated against satellite altimeter and in situ buoy data, showing the ability to reproduce the main historical climate signals with statistically robust trends. The wave climate models compare well to global satellite altimeter and in situ buoy data. When compared to traditional trend analyses, these models show that they can reproduce the main historical climate signals. The long-term datasets used in the study allow for a comprehensive description of the wave climate in the 20th and 21st centuries, and produce statistically significant trends [44]. The dataset is obtained by coupling the WaveWatch III (v6.07) model with CMIP6 models. The model is run under two IPCC Shared Socioeconomic Pathways (SSP1-26 and SSP5-85) [45], two models (ACCESS-CM2 and EC-EARTH3) and two parametrizations for SSP5-85 scenario (CDFAC1, CDFAC1.08) and one for the SSP1-26 scenario (CDFAC1.08). For the study, only the SSP5-85 IPCC representative greenhouse gas emission scenario is used (highest-end forcing pathway scenario in terms of greenhouse gas emission than SSP1-26 [46]). Therefore, there are four different future projections mixed under the worst scenario (see Section "Fluxu diagram"). This scenario is taken because last climatic data show that the worst scenario could be the most probable(see Section "Conclusions"). Several authors have investigated the evolution of different ocean parameters in higher emissions scenarios, e.g. [47] analysed the change on the wave energy resource potential in the Atlantic Coast of the Iberian Peninsula over different future time-frames under a high emission scenario and [48] analysed the climate change impact on waves in the Bay of Biscay under three potential future scenarios with a more thorough analysis for the higher emission scenario.

The dataset contains 3-hourly outputs in a global 0.5° × 0.5° spatial resolution, in the 2015–2100 period, with an added historical period (1985–2014). The variables used in our study are mean wave period (T_m), significant wave height (H_s), and wind speed at 10 metres high (U_{10}). These data are computed monthly with a confidence interval (CI) of 95% and Theil–Sen so that the trend computation is more robust [49], since this technique captures the medians of the signal [50]. Nevertheless, the graphics are plotted in a yearly scale with the Linear Regression Analysis in order to make trends more visual for the reader (Fig. 4).

Calibration method: CSIRO vs. ERA5

The CSIRO future projections were calibrated using ERA5 data to improve their accuracy. This calibration is necessary because the projections lack certain information that reanalysis data already has assimilated, such as meteorological ocean observations. In this study, the variables T_m, H_s, and U_{10} were corrected using the Quantile Matching (QM) technique [51]. This technique derives the calibration transfer

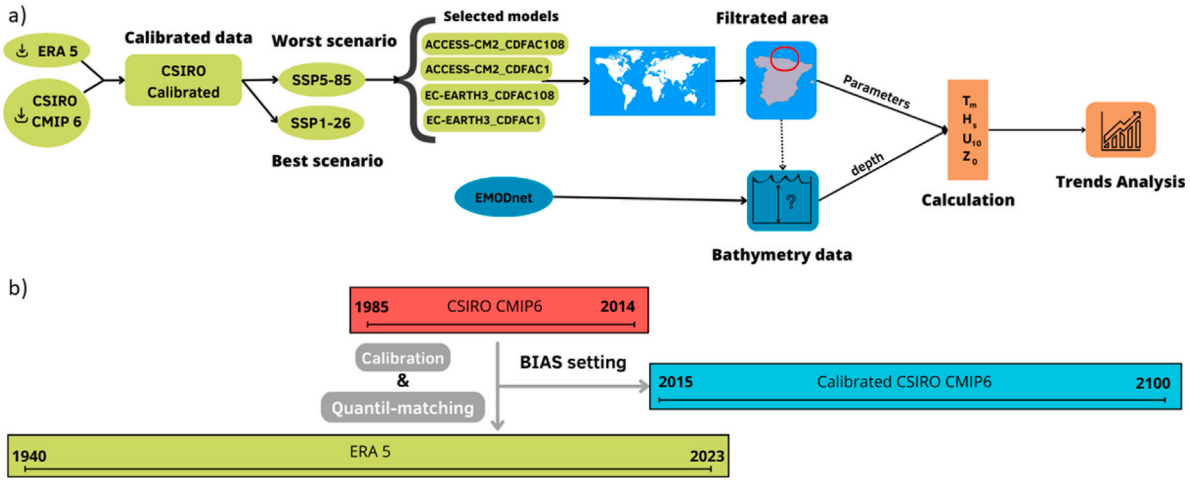

Fig. 2. Flux diagrams of: (a) Data synthesis, scenario and model selection, area and bathymetry filtration, and selected parameters trends computation; (b) Calibration of the CMIP6 versus ERA5 data set and future projection operations by QM.

function by calculating the percentile differences between the historical climate model and ERA5 reanalysis data both in the reference period (1985–2014). Then future projections of the climate model for the period 2015–2100 are adjusted using the transfer function obtained above for the reference period (see Fig. 3). The authors have previously used this technique in studies related to wave energy [52], wave energy converters [53] and wind energy [54] matching the quantiles in a direct way or even categorizing directional intervals of waves to obtain a unique transference function QM for each direction [12].

In this study, the technique was applied using the Quantile Mapping and Dressing (QMD) function of the Multivariate Bias Correction of Climate Model Outputs (MBC) R-package: [55]. This methodology is particularly important for climate change research, as it allows for more accurate projections of future climate conditions.

IEA 15-MW offshore wind turbine

The wind turbine model selected for the study (see report [56]) is the IEA 15-MW Offshore Reference Wind Turbine, developed by a collaboration between the National Renewable Energy Laboratory (NREL), the Technical University of Denmark (DTU) and the International Energy Agency (IEA). An important aspect of this turbine is that OpenFAST-based simulation and analysis using a semi-submersible platform [57] is supported, which fits the necessity of the location selected for this study.

This reference wind turbine is a IEC-Class IB direct-drive machine, with a rotor diameter of 240 m and a hub height of 150 m. The blade design was driven by the selection of the rotor diameter and a maximum tip speed of 95 m/s. The rated power is 15 MW and it has a 3 m/s cut-in wind speed, 10.59 m/s rated wind speed, and 25 m/s cut off wind speed as well as 5 rpm cut-in rotor speed and 7.56 rpm rated rotor speed [56]. The corresponding turbines power curve is shown in the supplementary material (Figure-S2).

Methodology

Sea roughness and wind vertical profile

To obtain the sea roughness value (z_0), Hsu Eq. (2) is used [58]. Here is the methodological novelty of this article: the use of wave data (height and period) to obtain the instantaneous sea roughness and, therefore, the vertical behaviour of wind speed in the atmospheric boundary layer. In this case, L is the wavelength and H_s is the representative wave height (both in metres) [33]. To use the Eqs. (1), (2), a deep water environment is considered where the ratio between the water depth and the wavelength d/L is bigger than 1/2 and the hyperbolic tangent is approximately equal to one [59].

$$L = \frac{gT^2}{2\pi}\sqrt{\tanh\left(\frac{4\pi^2 d}{T^2 g}\right)} \approx \frac{gT^2}{2\pi} \tag{1}$$

$$\frac{z_0}{H_s} = 1200\left(\frac{H_s}{L}\right)^{4.5} \tag{2}$$

Instead, to get the wind vertical profile, the wind shear or the variation in wind speed with height over water, the logarithmic Eq. (3) is used. As the height of the turbine is 150 m, and the available wind data is at 10 m, it is necessary to extrapolate the values to obtain data similar to reality in which instantaneous sea roughness (z_0) is taken into account [33].

$$\frac{U_{150}}{U_{10}} = \frac{\log(150/z_0)}{\log(10/z_0)} \tag{3}$$

Annual energy production and capacity factor

As the dataset used in the study has 3 hourly outputs, the Δt will be 3 h and the number of data in a year will be $N = 365.25 \cdot (24/3) = 2922$ data. This will help to calculate the Annual Energy Production (AEP) (Eq. (4)), and the Capacity Factor (CF) (Eq. (5)). With the first one (Eq. (4)), the total amount of electrical energy produced over a year is calculated; and the second one (Eq. (5)) shows the time percentage over a year that the turbine is running at its nominal or rated power (P_{rated}).

$$AEP = \sum_{i=1}^{N} P(U) \cdot \Delta t \tag{4}$$

$$CF = \frac{AEP}{P_{rated} \cdot 8760} \tag{5}$$

$P(U)$ is the function that relates, using the power curve, the produced power in function of wind speed at the hub height. A linear interpolation method is implemented in a discrete series of the IEA 15 MW wind turbine's power curve.

Future trends computation

Different visualization strategies and numerical values are used to show the trends:

1. All the trend figures are shown using yearly means, considering all the models equiprobable, given the importance of annual analysis for techno-economic issues in wind energy. This visualization is approximated via linear regression lines in Fig. 4.

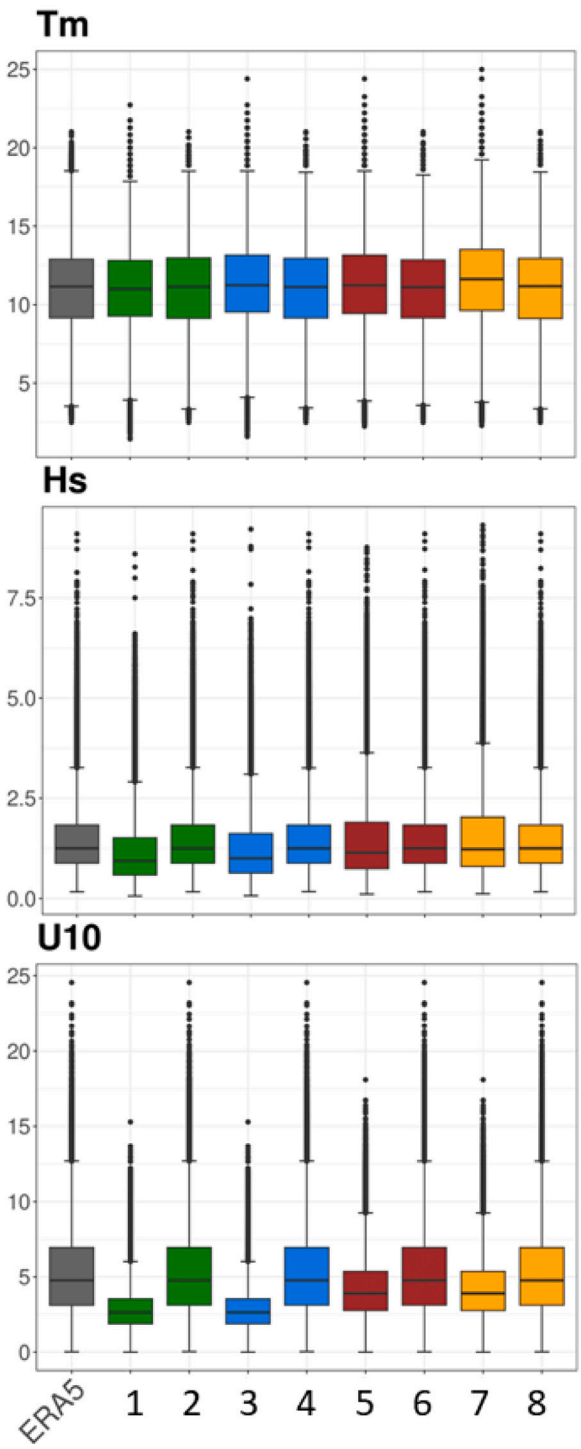

PARAMETER	SIMULATION		BIAS RATIO
T_m	1	historical_ACCESS.CM2_CDFAC1	0.01
	2	ACCESS.CM2_CDFAC1	0.00
	3	historical_ACCESS.CM2_CDFAC108	0.03
	4	ACCESS.CM2_CDFAC108	0.00
	5	historical_EC.EARTH3_CDFAC1	0.03
	6	EC.EARTH3_CDFAC1	0.00
	7	historical_EC.EARTH3_CDFAC108	0.06
	8	EC.EARTH3_CDFAC108	0.00
H_s	1	historical_ACCESS.CM2_CDFAC1	-0.20
	2	ACCESS.CM2_CDFAC1	0.00
	3	historical_ACCESS.CM2_CDFAC108	-0.15
	4	ACCESS.CM2_CDFAC108	0.00
	5	historical_EC.EARTH3_CDFAC1	-0.01
	6	EC.EARTH3_CDFAC1	0.00
	7	historical_EC.EARTH3_CDFAC108	0.06
	8	EC.EARTH3_CDFAC108	0.00
U_{10}	1	historical_ACCESS.CM2_CDFAC1	-0.46
	2	ACCESS.CM2_CDFAC1	0.00
	3	historical_ACCESS.CM2_CDFAC108	-0.46
	4	ACCESS.CM2_CDFAC108	0.00
	5	historical_EC.EARTH3_CDFAC1	-0.20
	6	EC.EARTH3_CDFAC1	0.00
	7	historical_EC.EARTH3_CDFAC108	-0.20
	8	EC.EARTH3_CDFAC108	0.00

Fig. 3. T_m, H_s and U_{10} validation boxplots, in pairs of the same colour, before (left side of the pair) and after (right side) calibration against ERA5.

2. For the exact numerical values of the trends and the corresponding tables, Theil–Sen method is applied on seasonal anomalies for monthly mean data. This technique offers more robust values with a CI of 95%. Annual and seasonal trends are computed by means of this method (see Tables 1,2).
3. Boxplots of 30 years (tridecades: 2011–2030; 2031–2060; 2061–2100) are also shown in some cases such as the Capacity Factor to avoid the interference of climatic patterns in the overall analysis [60], considering a equiprobable mix of the original models (see Fig. 5).

Flux diagram

The Fig. 2 shows the diagrams of how the data was managed. Firstly the calibration and bias correction was made by QM method. After that, the SSP5-85 pathway was selected as well as the two global climate models with two different parametrizations each one. Both selected models are on the top models with the most grid points statistically similar to ERA5-time series in Europe and North America. EC-Earth3, EC-EARTH-CONSORTIUM (Europe) [61], top 1 in Europe (67% similar) and top 3 in North America (64% similar); and ACCESS-CM2, Commonwealth Scientific and Industrial Research Organisation

Table 1
Summary of the Fig. 4, S3 and S4 trends, and their variation in 30-yr periods.

Parameter	Bottom CI slope (2.5%)	Central slope (50%)	Top CI slope (97.5%)	Mean variation per 30 yr (%)
T_m (s/10 yr)	−0.0037	−0.0542	−0.0411	−1.94%*
T_m winter	+0.0057	−0.0148	−0.0517	−0.45%
T_m summer	+0.0052	−0.0839	−0.1163	−3.50%
H_s (m/10 yr)	+0.0010	−0.0115	−0.0234	−2.75%
H_s winter	−0.0036	−0.0067	−0.0242	−1.17%*
H_s summer	+0.0049	−0.0062	−0.0558	−1.95%
U_{10} (m s^{-1}/10 yr)	+0.0014	−0.0137	−0.0349	−0.86%
U_{10} winter	−0.0097	−0.0279	−0.0111	−1.42%*
U_{10} summer	+0.0046	+0.0152	−0.0402	+1.19%
z_0 (m/10 yr)	+1.314E−09	+8.194E−08	−1.915E−06	+5.89%
z_0 winter	−6.957E−10	−7.002E−08	−3.471E−06	−3.08%*
z_0 summer	+8.626E−09	+2.001E−07	−1.116E−06	+19.99%

* Means that the slope is significant at a 95% CI.

(Australia) [62], top 8 in Europe (52% similar) and top 6 in North America (59% similar) [23]. Finally, the parameters were analysed in one legally possible grid-point limited by bathymetry and EU law as mentioned in Section "Study area".

Results

Validation vs. ERA5

The validation focused on the boxplot diagrams, which allow comparing different parameterizations and models with reference data ranging from 1985 to 2014 (see Section "Calibration method: CSIRO vs. ERA5") on the same graph. The results indicate similarity across the three initial variables analysed in this study, U, T_m and H_s. Note that the forth variable, z_0, is obtained by applying previous Eq. (2). The bias error [63] has been improved in all cases especially in the wind speed which is shown in the boxplot below (Fig. 3). The boxplot contains diagrams in pairs of the same colour (non calibrated on the left, calibrated on the right) for each of the simulations including parametrization that take part in the final data mix analysed in this paper. As it is shown, the calibrated boxplots show a significant improvement, mainly for the bias which is reduced to null in all the non-historical simulations, compared to the grey ERA5 first referential boxplot.

Future wind and wave trends

Fig. 4 shows the trends of parameters H_s and U_{10} in the future scenario, SSP5-85 IPCC, with period 2015–2100 for annual (a), winter (b) and summer (c) trends with its 95% CI. The corresponding figures of T_m and z_0 are shown in the supplementary material (Figures S3 and S4). The blue line is the 2.5% quantile, the grey and black one is the 50% quantile, or the median, and the red one is the 97.5% quantile.

The graphics trends are plotted using linear regression to make trends more visual. However, the tabular results are computed monthly with CI 95% and Theil–Sen in order to make trends more robust and reliable.

Table 1 shows, with a 95% CI, the top (97.5% quantile), the median (50% quantile) and the bottom (2.5% quantile) ramp values per decade, and, as can be seen in the last column, the relative change that this represents in a tridecade. The parameter with the major variation through a 30-year period (last column) is the sea roughness (z_0), giving its maximum change in summer. This is given the fact that the sea roughness values are barely noticeable for the human sight (it has values up to the order of 1E-7 m). Therefore, a small absolute change brings with it a large relative change. But this case is not very relevant because of the variation between positive and negative trends in the bottom and top CI slopes.

The main tendency of the parameters is to decrease. Despite the fact of the increasing trends of the bottom CI slope, its absolute values are about ten times less than the negative slope values of the top CI slope.

Table 2
Seasonal Theil–Sen analysis for each selected model in the worst greenhouse emission scenario (SSP5-85). NA value means that there is not any significant trend.

Model	Season	Generation power trend [kW/yr]		
		2.5% CI	50% CI	97.5% CI
ACCESS_1	Winter	−12.8085	−8.2169	−4.9280
ACCESS_108		−12.7651	−8.3043	−4.9432
EARTH_1		−2.7819	NA	5.1955
EARTH_108		−2.7548	NA	5.2080
ACCESS_1	Spring	−0.1464	NA	3.9233
ACCESS_108		−0.1480	NA	3.9432
EARTH_1		−4.4030	NA	0.2219
EARTH_108		−4.4115	NA	0.2224
ACCESS_1	Summer	1.3420	3.8900	4.3063
ACCESS_108		1.3317	3.8615	4.3082
EARTH_1		4.7930	6.4995	7.4592
EARTH_108		4.7646	6.4799	7.4346
ACCESS_1	Autumn	−7.8521	−4.1635	−0.8485
ACCESS_108		−7.8838	−4.1901	−0.8591
EARTH_1		−12.4398	−9.2734	−5.9179
EARTH_108		−12.4475	−9.2655	−5.9168

Therefore, the negative trends except for the z_0 have more influence. The reason for that z_0 positive change is the reduction of wave period (T_m) which also reduces the wavelength (L, (1)), increasing the wave slope (H/L) and therefore the roughness. Besides, it looks like the possibly most extreme events (Top CI values) are going to decrease during the 86 years time period prediction. This case is discussed in Section "Discussion". Overall, all the significant slopes are negative and the most of them are winter trends.

Future CF and AEP evolution

Fig. 5-a shows that the CF obtained is around 28%–29%. This is in agreement with a previous study of the authors [64], which shows a map of the Iberian Northern Coastline, with a potential CF of between 20%–28%. In the case of the present study, the CF is slightly higher due to the fact that, apart from having more advanced forecasting technology, the wind is analysed at a higher altitude (150 m), having higher wind quality and energy potential. Furthermore, it is in agreement with wind potential values given by Global Wind Atlas at that location (https://globalwindatlas.info/en) [65].

Having taken the mean annual CF values year by year for the boxplot, it can also be seen that the median and the upper end of the CF decrease slightly every 30 yr. The first tridecade or thirty years period is the period from 2011 to 2030; the second from 2031 to 2060; and the third and last from 2061 to 2100. If we analyse the annual evolution in the future, we obtain that the change for 2100 will be −1.9% of CF. In terms of energy generated, it is estimated that the AEP will decrease by −2.5 GWh by then.

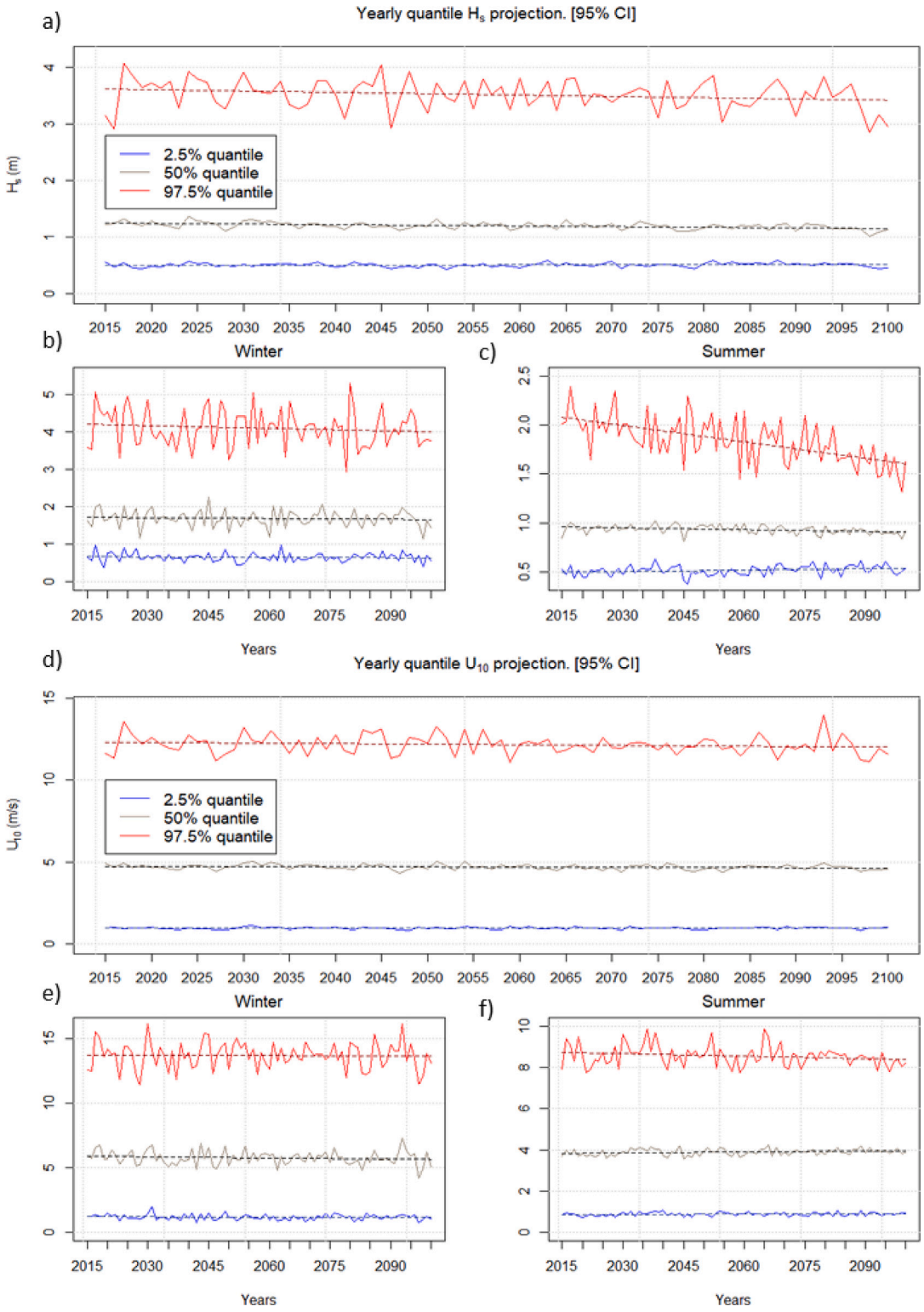

Fig. 4. (a) Year H_s projection-graphic with its 2.5%, 50% and 97.5% quantile trends. (b) H_s Winter projection-graphic with its trends. (c) H_s Summer projection-graphic with its trends. (d) Year U_{10} projection-graphic with its 2.5%, 50% and 97.5% quantile trends. (e) U_{10} Winter projection-graphic with its trends. (f) U_{10} Summer projection-graphic with its trends.

On the other hand, if we divide the CF analysis on the basis of the most influential seasons, winter [JFM] Fig. 5-b and summer [JAS] Fig. 5-c, in the future SSP5-85 IPCC scenario, the winter tridecades show that, as in the calculation of the global annual CF, it is reduced but obtaining much better results, 40%. In summer, on contrast, the CF increases as the tridecades go by, from 14% in the first tridecade to 15% in the third tridecade. Analysing the annual evolution in turn, in winter, the CF will decrease up to −2.9% by 2100 and in summer it will

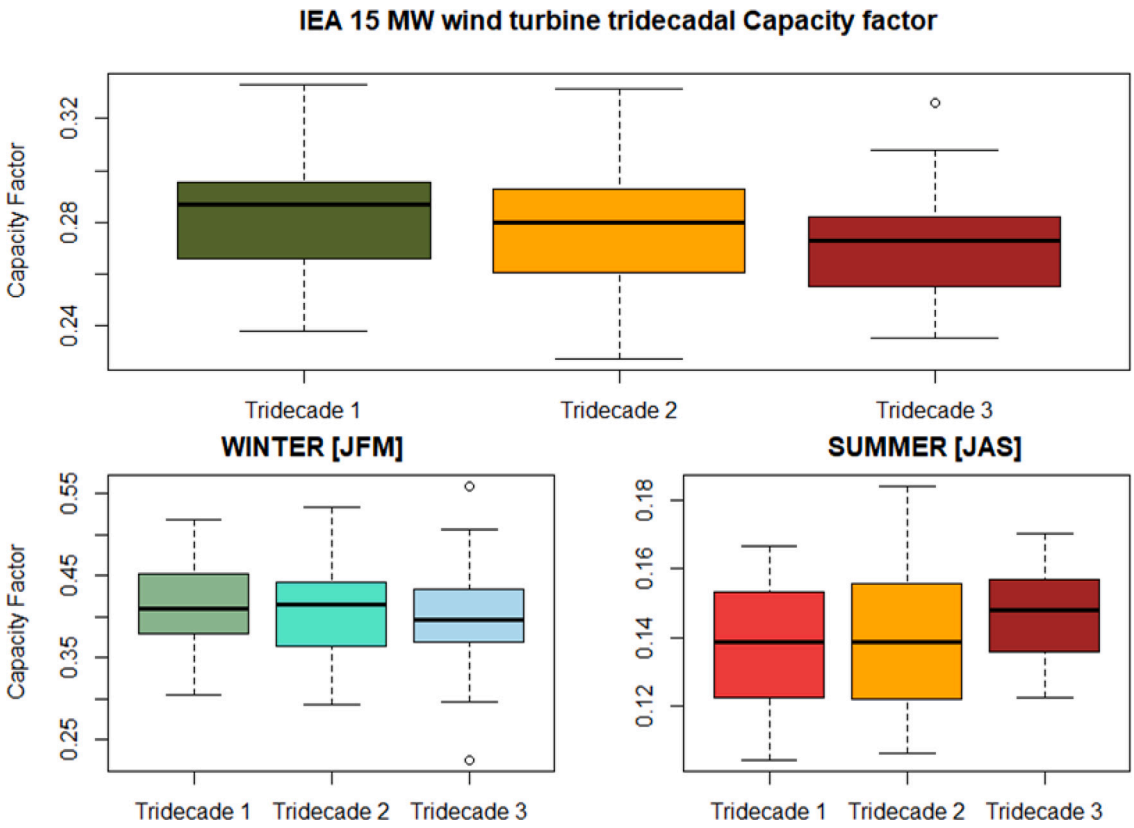

Fig. 5. (a) Annual average Capacity Factor tridecadal boxplot. (b) Annual winter [JFM] average Capacity Factor tridecadal boxplot. (c) Annual summer [JAS] average Capacity Factor tridecadal boxplot.

increase by +1.6%. Concerning energy, AEP, it will decrease by around −1 GWh in winter and increase by 0.5 GWh in summer respectively in the period of years analysed.

A more robust method based on Theil–Sen trend analysis within seasonal anomalies monthly for each model shows the following generation power trends, which are coherent in comparison with the previous 30 yr boxplots. There are some NA values in the table because there are not any significant values since the top and bottom slopes trends differ.

As seen in the tri-decades boxplot Fig. 5, the generation power significant trends on winter are negative and in summer positive. On the other hand, except for summer season, all the bottom CI (2.5%) values are decreasing trends whereas nothing relevant can be deducted with the top CI (97.5%) values. It is also remarkable that there are decreasing trends on autumn which may mean a smoother change between seasons.

Extreme waves and winds

Another important result for future projections is the behaviour of extreme events, which can be related to higher fatigue and loads in the future for different floating structures [66], and a reduction of the life cycle of the wind turbines. Given the lack of general definition of extreme event, the 99% quantile has considered here as a first approximation. Fig. 6 show these projections computing the CI of the slopes for 99% quantile events in both wave and wind, the two main parameters when it comes to energy flux and structure loads. In each parameter, the blue line encompasses the 99% quantile of the annual winter events, the red line the 99% quantile of the annual summer events and the grey line the 99% quantile of the total annual events, considering 99% quantile as a definition of extreme.

As seen in Fig. 5, the phenomenon of extreme events defined at 99% quantiles mostly tends to decrease. The most affected parameter is the summer significant wave height which is predicted to decrease more than a 8% in a thirty years period. As the summer season is not such a extreme season in the scope of the H_s, the diminution of the extreme events will not be noticed as in other seasons. The U_{10} winter trend remains practically constant but always tending to increase (+0.03% in a tridecade) being the only one with positive changes; the same occurs to H_s on winter which in this case tends to decrease (−0.86% in a tridecade).

Discussion

The results confirm what other papers have already shown: the expected slight negative changes in the north Atlantic [67] and Bay of Biscay [68] in the parameters analysed for future decades. This annually negligible and small reduction for winter projected for the 21th century in wind energy production is a paradigmatic result, since previous investigations in the Iberian Peninsula for historical offshore wind energy production using ERA5 (1950–2010) show relevant increments in wind energy [54]. This increments are even higher for wave height and wave energy if 20th century is taken into account calibrating ERA20C reanalysis in the Bay of Biscay [52], the West of Ireland [10], Iceland [11], or even South Hemisphere in Chile [12].

As mentioned, the novelty of the methodology is in the determination of the sea state according to the instantaneous roughness (depending on wave height and period) to raise the wind speed at 10 m to the hub height of the turbine with the corresponding vertical profile. The significant increments of 10%–15% created in the past a gradually rougher sea condition, which would reduce the wind speed at hub height of wind turbines. The authors show that this effect of hypothetical rougher seas due to global warming will not be the case in the future evolution of the Bay of Biscay. Other global studies, mainly given by the changes in the frequency of extreme weather events or the hemispheric asymmetry can detect other locations where the future

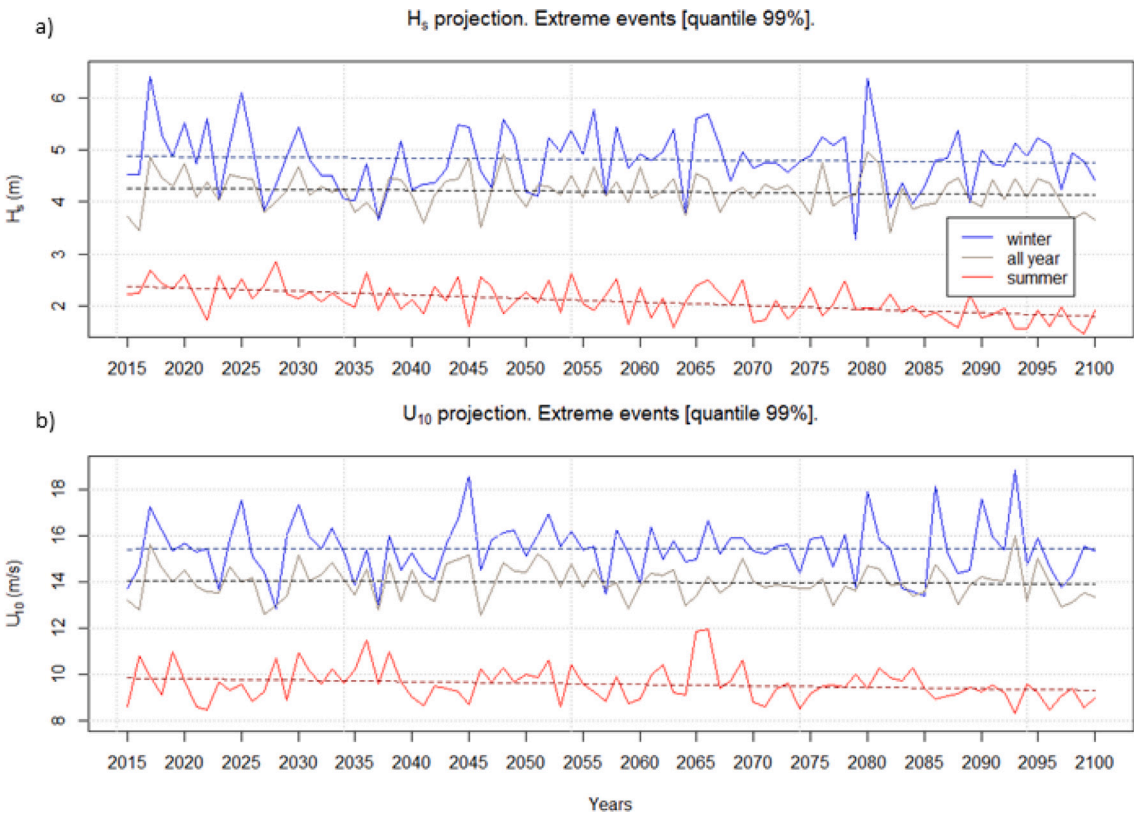

Fig. 6. (a) Yearly H_s projection graphic with its yearly, winterly and summerly 99% quantile trends. (b) Yearly U_{10} projection graphic with its yearly, winterly and summerly 99% quantile trends.

variations are stronger [69,70]. The climatic and physical explanation of this phenomenon is out of scope of this paper.

This future small or negligible variations are repeated for extreme wind and waves, but the positive trend for extreme wind speed at 99% quantile together with the reduction of extreme waves, implies that the influence of local winds is weakening in the future in favour of swell waves. This implies a more regular wave frequency and controllable floating turbine [71], which, together with a constant roughness, would not affect the fatigue loads of the structure like in the past projections [72].

The influence of the hub height in future power production trends should be also discussed, given that turbines of 5 MW and 100 m hub height have shown even smaller production variations. According to error theory, and considering the Wind Power Density (WPD) proportional to U^3, the relative error of WPD, $dWPD_r = \frac{dWPD}{WPD} = \frac{3U^2dU}{U^3} = 3dU_r$, is three times the relative error of wind speed dU_r, that is, a variation of 1% of wind speed during decades means a variation of 3% for natural wind power. This is the main theoretical reason why small variations or insignificant variations of wind speed can affect the real production of the wind turbine, mainly between the cut-in speed and rated wind speed of the turbine [33] (see Section "IEA 15-MW offshore wind turbine" or Figure-S2 of the supplementary material), the part of the power curve governed by the cubic behaviour between power and wind speed. Thus, the most robust analysis in the Table 2 for power in kW and for each future model, shows more relevant trends for all the seasons, with exception of Spring. This seasonal long-term variation emphasizes the need of ocean energy harvesting to regulate the electricity output, mechanically [73], or using triboelectric nanogenerator arranged longitudinally under water [74].

The studied period for CF is 30 yr (one tridecade), as shown in Fig. 5, that is, the database includes ≈90,000 3-hourly cases for each model. For the climatological standards, this reference period corresponds to the current guidelines by the World Meteorological Organization [75], or institutes such as the Copernicus Climate Change Service [76]. Only the median in the boxplot of the last tridecade shows for winter a relevant reduction, constituting a climatically more significant information than the typical slope computation of variation per decade. Anyway, this tridecade analysis is coherent with the main trends per decade computed using Theil–Sen method and corresponding uncertainties. This uni-parametric estimations can be improved in the future using multi-parametric uncertainties [77,78].

Similarly, the economic losses generated by the main negative winter trends have been calculated since the changes in energy production are seasonal and the negative winter trends are significant as seen in Table 1. For this purpose, it has been taken into account that the Levelized Cost of Energy (LCOE) is currently higher than 160 EUR/MWh on the Cantabrian Coast according to [79] with any floating and anchoring method. Maintaining this value until 2100, despite the fact that some experts report that by 2050 the LCOE will decrease around 35%–41% [80], and without taking inflation into account, by the year 2100 it would reduce generation during winter season, the most productive season, between 100,000–200,000 EUR.

Conclusions

CMIP6 is the last configuration of the global climate models designed to estimate future climate projection. CSIRO offers pioneering metocean data, in which a worldwide atmospheric-oceanic coupling model has been run to estimate the corresponding wave data, in a way consistent with the wind and wave data from the global climate model. Here is the methodological novelty of this approach: wave period and height determines the instantaneous sea roughness which establishes the behaviour of the wind vertical profile at the hub height of the turbine.

The selected gridpoint and its surrounding area, with similar characteristics, have an adequate but decreasing energy potential just visualizing the descending trends of T_m, H_s, U_{10}, z_0, and the AEP and

CF of the wind turbine using its real power curve in future SSP5-85 IPCC scenario with the highest CO2 emissions by 2100. The plotted linear regressions have shown the slightly decreasing tendency of the parameters in winter and the mainly decreasing trends of the most extreme events.

For the energy production of the turbine, although the variations for turbines smaller than 5 MW has been found insignificant even at the worst scenario [81], this reduction for the 15 MW turbine implies a corresponding statistically significant reduction in annual CF of around −2% by 2100 for SSP5-85. This reduction is insignificant for the middle and low emission scenarios, but last climatic data show that the worst scenario considered here could be more probable than the middle one. The most likely climate scenario is that global temperatures will rise by about 2.7 °C by 2100. This is the middle of the road scenario, also known as SSP3-7.0, near SSP5-85, outlined in the Intergovernmental Panel on Climate Change (IPCC) Sixth Assessment Report (AR6) [82].

Under this scenario, greenhouse gas emissions continue to increase throughout the century, reaching a peak around 2080 before slowly declining. This leads to a steady increase in global temperatures, with the possibility of reaching 3 degrees Celsius (5.4 degrees Fahrenheit) by the end of the century.

Given the universal nature of the presented methods, it would be possible to perform the same analysis in other marine regions around the world to analyse the offshore wind energy potential future evolution. Future work can also analyse the energy production of a wave energy converter since wave data are available, and even the evolution of the hybridation of both marine sources, wind and wave [83], considering co-location indexes [84], covariance analysis and the algebra of index decomposition developed by the authors for other energetic applications and also in the analysis of poverty and energy poverty [85]. Solar-wind-wave energy hybridation can be another approximation in this sense [86].

CRediT authorship contribution statement

Hodei Ezpeleta: Writing – review & editing, Writing – original draft, Visualization, Validation, Supervision, Software, Resources, Methodology, Investigation, Formal analysis, Data curation, Conceptualization. **Alain Ulazia:** Writing – review & editing, Writing – original draft, Funding acquisition, Formal analysis, Data curation, Conceptualization. **Gabriel Ibarra-Berastegi:** Writing – review & editing, Writing – original draft, Supervision, Software, Resources, Methodology, Investigation. **Jon Sáenz:** Writing – review & editing, Writing – original draft, Supervision, Software, Project administration, Investigation, Funding acquisition. **Sheila Carreno-Madinabetia:** Writing – review & editing, Writing – original draft, Validation, Supervision, Software, Resources, Formal analysis. **Oihana Aristondo:** Writing – original draft, Validation, Resources.

Declaration of competing interest

The authors declare that they have no known competing financial interests or personal relationships that could have appeared to influence the work reported in this paper.

Data availability

Data will be made available on request.

Acknowledgements

This study is part of project PID2020-116153RB-I00 funded by Ministerio de Ciencia e Innovación/Agencia Estatal de Investigación MCIN/AEI/10.13039/501100011033. This study was part of the TED2021-132109B-C21 research project funded by MCIN/AEI/10.13039/501100011033 and the European Union NextGenerationEU/PRTR. The authors acknowledge funding from the University of the Basque Country through research group calls (UPV/EHU, GIU20/08).

Appendix A. Supplementary data

Supplementary material related to this article can be found online at https://doi.org/10.1016/j.seta.2024.103776.

References

[1] Li Y, Huang X, Tee KF, Li Q, Wu X-P. Comparative study of onshore and offshore wind characteristics and wind energy potentials: A case study for southeast coastal region of China. Sustain Energy Technol Assess 2020;39:100711.
[2] Council of the European Union. Climate change. 2023, URL https://www.consilium.europa.eu/en/policies/climate-change/, Accessed on October 7, 2023, No date.
[3] Colmenar-Santos A, Perera-Perez J, Borge-Diez D, dePalacio Rodríguez C. Offshore wind energy: A review of the current status, challenges and future development in Spain. Renew Sustain Energy Rev 2016;64:1–18.
[4] Yang C, Hou X, Chang S. A synchronous placement and size-based multi-objective optimization method for heat dissipation design on antenna module of space solar power satellite. Sustain Energy Technol Assess 2021;45:101183.
[5] Yang C, Yu Q. Placement and size-oriented heat dissipation optimization for antenna module in space solar power satellite based on interval dimension-wise method. Aerosp Sci Technol 2023;134:108155.
[6] Görmüş T, Aydoğan B, Ayat B. Offshore wind power potential analysis for different wind turbines in the Mediterranean Region, 1959–2020. Energy Convers Manage 2022;274:116470.
[7] Commission E. Press release: European green deal: Commission adopts new circular economy action plan - questions and answers. 2020, URL https://ec.europa.eu/commission/presscorner/detail/en/ip_20_2096, Accessed on October 7, 2023.
[8] Vázquez A, Izquierdo U, Enevoldsen P, Andersen F-H, Blanco JM. A macroscale optimal substructure selection for Europe's offshore wind farms. Sustain Energy Technol Assess 2022;53:102768.
[9] Ibarra-Berastegi G, Saénz J, Esnaola G, Ezcurra A, Ulazia A. Short-term forecasting of the wave energy flux: Analogues, random forests, and physics-based models. Ocean Eng 2015;104:530–9.
[10] Penalba M, Ulazia A, Ibarra-Berastegui G, Ringwood J, Sáenz J. Wave energy resource variation off the west coast of Ireland and its impact on realistic wave energy converters' power absorption. Appl Energy 2018;224:205–19.
[11] Penalba M, Ulazia A, Saénz J, Ringwood JV. Impact of long-term resource variations on wave energy Farms: The Icelandic case. Energy 2020;192:116609.
[12] Ulazia A, Penalba M, Rabanal A, Ibarra-Berastegi G, Ringwood J, Sáenz J. Historical evolution of the wave resource and energy production off the chilean coast over the 20th century. Energies 2018;11(9):2289.
[13] Kalogeri C, Galanis G, Spyrou C, Diamantis D, Baladima F, Koukoula M, Kallos G. Assessing the European offshore wind and wave energy resource for combined exploitation. Renew Energy 2017;101:244–64.
[14] Plan de Ordenación del espacio marítimo. 2023, URL https://www.miteco.gob.es/es/costas/temas/proteccion-medio-marino/ordenacion-del-espacio-maritimo.html, Accessed: 2023-11-30.
[15] Pérez MG. El plan de ordenación de espacios marítimos de la demarcación marina noratlántica. In: Planificación del espacio marino: aplicación en españa de la directiva marco 2014/89/UE. RDU; 2022, p. 263–314.
[16] Abramic A, Mendoza AG, Haroun R. Introducing offshore wind energy in the sea space: Canary islands case study developed under Maritime Spatial Planning principles. Renew Sustain Energy Rev 2021;145:111119.
[17] Castro-Santos L, Bento AR, Silva D, Salvação N, Guedes Soares C. Economic feasibility of floating offshore wind farms in the north of Spain. J Mar Sci Eng 2020;8(1):58.
[18] Diez-Caballero K, Troiteiro S, García-Alba J, Vidal JR, González M, Ametller S, Juan R. Environmental compatibility of the parc tramuntana offshore wind project in relation to marine ecosystems. J Mar Sci Eng 2022;10(7):898.
[19] Martinez A, Iglesias G. Wind resource evolution in Europe under different scenarios of climate change characterised by the novel Shared Socioeconomic Pathways. Energy Convers Manage 2021;234:113961. http://dx.doi.org/10.1016/j.enconman.2021.113961.
[20] Martinez A, Iglesias G. Global wind energy resources decline under climate change. Energy 2024;288:129765. http://dx.doi.org/10.1016/j.energy.2023.129765.
[21] Jung C, Schindler D. A review of recent studies on wind resource projections under climate change. Renew Sustain Energy Rev 2022;165:112596. http://dx.doi.org/10.1016/j.rser.2022.112596.
[22] Ibarra-Berastegui G, Sáenz J, Ulazia A, Sáenz-Aguirre A, Esnaola G. CMIP6 projections for global offshore wind and wave energy production (2015–2100). Sci Rep 2023;13(1):18046. http://dx.doi.org/10.1038/s41598-023-45450-3.
[23] Martinez A, Iglesias G. Climate change impacts on wind energy resources in North America based on the CMIP6 projections. Sci Total Environ 2022;806:150580. http://dx.doi.org/10.1016/j.scitotenv.2021.150580.

[24] Fournier A, Martinez A, Iglesias G. Impacts of climate change on wind energy potential in Australasia and South-East Asia following the Shared Socioeconomic Pathways. Sci Total Environ 2023;882:163347. http://dx.doi.org/10.1016/j.scitotenv.2023.163347.
[25] Martinez A, Murphy L, Iglesias G. Evolution of offshore wind resources in Northern Europe under climate change. Energy 2023;269:126655. http://dx.doi.org/10.1016/j.energy.2023.126655.
[26] Zhang S, Li X. Future projections of offshore wind energy resources in China using CMIP6 simulations and a deep learning-based downscaling method. Energy 2021;217:119321. http://dx.doi.org/10.1016/j.energy.2020.119321.
[27] Martinez A, Iglesias G. Climate-change impacts on offshore wind resources in the Mediterranean Sea. Energy Convers Manage 2023;291:117231. http://dx.doi.org/10.1016/j.enconman.2023.117231.
[28] Qian H, Zhang R. Future changes in wind energy resource over the Northwest Passage based on the CMIP6 climate projections. Int J Energy Res 2021;45(1):920–37. http://dx.doi.org/10.1002/er.5997.
[29] Hahmann AN, García-Santiago O, Peña A. Current and future wind energy resources in the North Sea according to CMIP6. Wind Energy Sci 2022;7(6):2373–91. http://dx.doi.org/10.5194/wes-7-2373-2022.
[30] Miao H, Xu H, Huang G, Yang K. Evaluation and future projections of wind energy resources over the Northern Hemisphere in CMIP5 and CMIP6 models. Renew Energy 2023;211:809–21. http://dx.doi.org/10.1016/j.renene.2023.05.007.
[31] Moradian S, Akbari M, Iglesias G. Optimized hybrid ensemble technique for CMIP6 wind data projections under different climate-change scenarios. Case study: United Kingdom. Sci Total Environ 2022;826:154124. http://dx.doi.org/10.1016/j.scitotenv.2022.154124.
[32] Basak D, Nagababu G, Puppala H, Patel J, Kumar SVVA. Foreseeing the spatio-temporal offshore wind energy potential of India using a differential weighted ensemble created using CMIP6 datasets. Reg Stud Mar Sci 2023;65:103066. http://dx.doi.org/10.1016/j.rsma.2023.103066.
[33] Manwell JF, McGowan JG, Rogers AL. Wind energy explained: theory, design and application. John Wiley & Sons; 2010.
[34] Tedeschi E, Santos-Mugica M. Modeling and control of a wave energy farm including energy storage for power quality enhancement: The bimep case study. IEEE Trans Power Syst 2013;29(3):1489–97.
[35] Ibarra-Berastegi G, Sáenz J, Ulazia A, Serras P, Esnaola G, Garcia-Soto C. Electricity production, capacity factor, and plant efficiency index at the Mutriku wave farm (2014–2016). Ocean Eng 2018;147:20–9.
[36] Barooni M, Ashuri T, Velioglu Sogut D, Wood S, Ghaderpour Taleghani S. Floating offshore wind turbines: Current status and future prospects. Energies 2022;16(1):2.
[37] Lavalle C, Gomes CR, Baranzelli C, e Silva FB. Coastal zones, policy alternatives impacts on European Coastal Zones, 2050. 2000.
[38] Butterfield S, Musial W, Jonkman J, Sclavounos P. Engineering challenges for floating offshore wind turbines. Tech. rep., Golden, CO (United States: National Renewable Energy Lab.(NREL); 2007.
[39] EMODnet. European Marine observation and data network (EMODnet). 2023, URL https://emodnet.ec.europa.eu/en.
[40] Hersbach H, Peubey C, Simmons A, Berrisford P, Poli P, Dee D. ERA-20CM: A twentieth-century atmospheric model ensemble. Q J R Meteorol Soc 2015;141(691):2350–75.
[41] ECMWF. ECMWF - European centre for medium-range weather forecasts. 2023, URL https://www.ecmwf.int/.
[42] Peuch V-H, Engelen R, Rixen M, Dee D, Flemming J, Suttie M, Ades M, Agustí-Panareda A, Ananasso C, Andersson E, et al. The copernicus atmosphere monitoring service: From research to operations. Bull Am Meteorol Soc 2022;103(12):E2650–68.
[43] Meucci A, Young I, Hemer M, Trenham C. CSIRO data collection. 2023, URL https://data.csiro.au/collection/csiro:53176.
[44] Meucci A, Young IR, Hemer M, Trenham C, Watterson IG. 140 Years of global ocean wind-wave climate derived from CMIP6 ACCESS-CM2 and EC-Earth3 GCMs: Global trends, regional changes, and future projections. J Clim 2023;36(6):1605–31.
[45] Riahi K, Van Vuuren DP, Kriegler E, Edmonds J, O'neill BC, Fujimori S, Bauer N, Calvin K, Dellink R, Fricko O, et al. The Shared Socioeconomic Pathways and their energy, land use, and greenhouse gas emissions implications: An overview. Glob Environ Change 2017;42:153–68.
[46] Rusu L. The near future expected wave power in the coastal environment of the Iberian Peninsula. Renew Energy 2022;195:657–69. http://dx.doi.org/10.1016/j.renene.2022.06.047.
[47] Majidi AG, Ramos V, Giannini G, Santos PR, das Neves L, Taveira-Pinto F. The impact of climate change on the wave energy resource potential of the Atlantic Coast of Iberian Peninsula. Ocean Eng 2023;284:115451.
[48] Charles E, Idier D, Delecluse P, Déqué M, Le Cozannet G. Climate change impact on waves in the Bay of Biscay, France. Ocean Dyn 2012;62:831–48.
[49] Theil H. A rank-invariant method of linear and polynomial regression analysis. Indag Math 1950;12(85):173.
[50] Sen PK. Estimates of the regression coefficient based on Kendall's tau. J Amer Stat Assoc 1968;63(324):1379–89.
[51] Cannon AJ, Sobie SR, Murdock TQ. Bias correction of GCM precipitation by quantile mapping: how well do methods preserve changes in quantiles and extremes? J Clim 2015;28(17):6938–59.
[52] Ulazia A, Penalba M, Ibarra-Berastegui G, Ringwood J, Saénz J. Wave energy trends over the Bay of Biscay and the consequences for wave energy converters. Energy 2017;141:624–34.
[53] Ulazia A, Penalba M, Ibarra-Berastegui G, Ringwood J, Sáenz J. Reduction of the capture width of wave energy converters due to long-term seasonal wave energy trends. Renew Sustain Energy Rev 2019;113:109267.
[54] Carreno-Madinabeitia S, Ibarra-Berastegi G, Sáenz J, Ulazia A. Long-term changes in offshore wind power density and wind turbine capacity factor in the Iberian Peninsula (1900–2010). Energy 2021;226:120364.
[55] Cannon AJ. MBC: Multivariate bias correction. 2023, https://CRAN.R-project.org/package=MBC.
[56] Gaertner E, Rinker J, Sethuraman L, Zahle F, Anderson B, Barter GE, Abbas NJ, Meng F, Bortolotti P, Skrzypinski W, et al. IEA wind TCP task 37: definition of the IEA 15-megawatt offshore reference wind turbine. Tech. rep., National Renewable Energy Lab.(NREL), Golden, CO (United States); 2020.
[57] Allen C, Viscelli A, Dagher H, Goupee A, Gaertner E, Abbas N, Hall M, Barter G. Definition of the UMaine VolturnUS-S reference platform developed for the IEA wind 15-megawatt offshore reference wind turbine. Tech. rep., Golden, CO (United States); Univ. of . . . : National Renewable Energy Lab.(NREL); 2020.
[58] Hsu S. Estimating overwater friction velocity and exponent of power-law wind profile from gust factor during storms. J Waterw Port Coast Ocean Eng 2003;129(4):174–7.
[59] Sundar V. Ocean wave mechanics: Applications in marine structures. John Wiley & Sons; 2017.
[60] von Trentini F, Aalbers EE, Fischer EM, Ludwig R. Comparing interannual variability in three regional single-model initial-condition large ensembles (SMILEs) over Europe. Earth Syst Dyn 2020;11(4):1013–31.
[61] (EC-Earth) E-EC. EC-Earth-Consortium EC-Earth3 model output prepared for CMIP6 scenarioMIP ssp585. 2019, http://dx.doi.org/10.22033/ESGF/CMIP6.4912.
[62] Dix M, Bi D, Dobrohotoff P, Fiedler R, Harman I, Law R, Yang R. CSIRO-ARCCSS access-CM2 model output prepared for CMIP6 ScenarioMIP ssp126 (version 20200512). Earth Syst Grid Fed 2019. http://dx.doi.org/10.22033/ESGF/CMIP64319.
[63] WWRP/WGNE Joint Working Group on Forecast Verification Research Centre for Australian Weather and Climate Research. Verification of forecast and climate projections methods. 2015, URL https://www.cawcr.gov.au/projects/verification/.
[64] Ulazia A, Saenz J, Ibarra-Berastegui G. Sensitivity to the use of 3DVAR data assimilation in a mesoscale model for estimating offshore wind energy potential. A case study of the Iberian northern coastline. Appl Energy 2016;180:617–27.
[65] Badger J, Hahmann A, Larsén XG, Badger M, Kelly M, Olsen BT, Mortensen NG. The Global Wind Atlas: An EUDP project carried out by DTU wind energy. 2015.
[66] Lu F, Long K, Diaeldin Y, Saeed A, Zhang J, Tao T. A time-domain fatigue damage assessment approach for the tripod structure of offshore wind turbines. Sustain Energy Technol Assess 2023;60:103450. http://dx.doi.org/10.1016/j.seta.2023.103450.
[67] Lobeto H, Menendez M, Losada IJ. Future behavior of wind wave extremes due to climate change. Sci Rep 2021;11(1):7869.
[68] Bernardino M, Goncalves M, Guedes Soares C. Marine climate projections toward the end of the twenty-first century in the north Atlantic. J Offshore Mech Arct Eng 2021;143(6):061201.
[69] Reguero BG, Losada IJ, Méndez FJ. A recent increase in global wave power as a consequence of oceanic warming. Nat Commun 2019;10(1):1–14.
[70] Patra A, Min S-K, Son S-W, Yeh S-W. Hemispheric asymmetry in future wave power changes: Seasonality and physical mechanisms. J Geophys Res: Oceans 2021;126(12):e2021JC017687.
[71] Lackner MA. Controlling platform motions and reducing blade loads for floating wind turbines. Wind Eng 2009;33(6):541–53.
[72] Saenz-Aguirre A, Ulazia A, Ibarra-Berastegi G, Saenz J. Floating wind turbine energy and fatigue loads estimation according to climate period scaled wind and waves. Energy Convers Manage 2022;271:116303. http://dx.doi.org/10.1016/j.enconman.2022.116303.
[73] Zhao L-C, Zou H-X, Wei K-X, Zhou S-X, Meng G, Zhang W-M. Mechanical intelligent energy harvesting: from methodology to applications. Adv Energy Mater 2023;13(29):2300557.
[74] Du Y, Tang Q, Fu S, Shan C, Zeng Q, Guo H, Hu C. Chain-flip plate triboelectric nanogenerator arranged longitudinally under water for harvesting water wave energy. Nano Res 2023;16(9):11900–6.
[75] WMO guidelines on the calculation of climate normals. Tech. rep. WMO-No. 1203, Geneva, Switzerland: World Meteorological Organization; 2017, p. 18.
[76] Changing the reference period from 1981–2020 to 1991–2020 for the C3s climate bulletin. 2021, URL https://climate.copernicus.eu/sites/default/files/2021-02/C3S_Climate_Bulletin_change_from_1981-2010_to_1991-2020_reference_period_v08-Feb-20_all.pdf.
[77] Yang C, Xia Y. Interval Pareto front-based multi-objective robust optimization for sensor placement in structural modal identification. Reliab Eng Syst Saf 2024;242:109703.

[78] Yang C. Interval strategy-based regularization approach for force reconstruction with multi-source uncertainties. Comput Methods Appl Mech Engrg 2024;419:116679.
[79] Martinez A, Iglesias G. Mapping of the levelised cost of energy for floating offshore wind in the European Atlantic. Renew Sustain Energy Rev 2022;154:111889.
[80] Wiser R, Jenni K, Seel J, Baker E, Hand M, Lantz E, Smith A. Expert elicitation survey on future wind energy costs. Nat Energy 2016;1(10):1–8.
[81] Ibarra-Berastegui G, Sáenz J, Ulazia A, Sáenz-Aguirre A, Esnaola G. CMIP6 projections for global offshore wind and wave energy production (2015–2100). Sci Rep 2023;13(1):18046.
[82] Intergovernmental Panel on Climate Change. Climate change 2021: The physical science basis. Working group i contribution to the sixth assessment report of the intergovernmental panel on climate change. 2021, URL https://www.ipcc.ch/report/ar6/wg1/.
[83] Saenz-Aguirre A, Saenz J, Ulazia A, Ibarra-Berastegui G. Optimal strategies of deployment of far offshore co-located wind-wave energy farms. Energy Convers Manage 2022;251:114914.
[84] Ulazia A, Sáenz J, Saenz-Aguirre A, Ibarra-Berastegui G, Carreno-Madinabeitia S. Paradigmatic case of long-term colocated wind–wave energy index trend in Canary Islands. Energy Convers Manage 2023;283:116890.
[85] Aristondo O. 31. The decomposition of unidimensional poverty measures. Res Handb Meas Poverty Deprivation 2023;326.
[86] Bi C, Law AW-K. Co-locating offshore wind and floating solar farms–effect of high wind and wave conditions on solar power performance. Energy 2023;266:126437.